Vibronically coherent speed-up of the excitation energy transfer in the Fenna-Matthews-Olson complex

P. Nalbach, C. A. Mujica-Martinez, and M. Thorwart
I. Institut für Theoretische Physik, Universität Hamburg, Jungiusstraße 9, 20355 Hamburg, Germany
and The Hamburg Centre for Ultrafast Imaging, Luruper Chaussee 149, 22761 Hamburg, Germany
(Received 18 January 2014; revised manuscript received 16 June 2014; published 10 February 2015)

We show that underdamped molecular vibrations fuel the efficient excitation energy transfer in the Fenna-Matthews-Olson molecular aggregate under realistic physiological conditions. By employing an environmental fluctuation spectral function derived from experiments, we obtain numerically exact results for the exciton quantum dynamics in the presence of underdamped vibrationally coherent quantum states. Assuming the prominent 180-cm^{-1} vibrational mode to be underdamped, additional coherent transport channels for the excitation energy transfer open up and we observe an increase of the transfer speed towards the reaction center by up to 24%.

DOI: 10.1103/PhysRevE.91.022706 PACS number(s): 82.37.Vb, 03.65.Yz, 82.53.−k

I. INTRODUCTION

Recent experiments on the ultrafast exciton dynamics in photoactive biomolecular complexes have sparked renewed interest in the longstanding question whether nontrivial quantum coherence effects exist in natural biological systems under physiological conditions, and, if so, whether they have any functional significance. Photosynthesis [1] starts with the harvest of a photon by a pigment and the formation of a tightly bound electron-hole pair. After the exciton has been formed in the antenna complexes, its energy is transferred nonradiatively by a Coulomb dipolar coupling to the reaction center (RC), where the charge separation is initiated. Thereby, the partial delocalization of the Frenkel exciton states over neighboring pigments is common [2,3].

Recently, Engel *et al.* [4,5] have reported long-lasting beating signals in time-resolved optical two-dimensional spectra of the Fenna-Matthews-Olson (FMO) complex [6–8] and interpreted them as evidence for quantum coherent energy transfer via delocalized exciton states. The FMO complex is a trimer with eight bacteriochlorophyll (BChl) molecular sites in each monomer. Figure 1 sketches the structural arrangement of the seven main BChl molecules, the delocalized Frenkel excitons, and the prevailing energy passageways. Its main function is the transfer of energy from the chlorosome, i.e., the main antennae complex, towards the reaction center in green sulfur bacteria. Engel *et al.* [4] speculated that the observed coherence is integral to and fuels the fast and efficient energy transfer through this complex. These reports have boosted ongoing research to answer two questions: first, how can quantum coherence prevail over the observed long times of more than 300 fs at physiological temperatures in its strongly fluctuating polar solvent, and, second, is the efficient energy transfer fuelled by coherence?

Theoretical modeling of the real-time quantum transfer dynamics is difficult due to the tremendous complexity of the system. Also, within the framework of open quantum systems, the nonstandard spectral distributions of the fluctuations render the analysis challenging. Standard Redfield-type approaches are based on the assumption of a weak-damping and a Markovian (single-phonon) approximation whose validity is not clear *a priori* [9–12]. The numerically exact treatment of the FMO model with seven localized and interacting sites and a measured fluctuational power spectrum [13,14] including a strongly localized Huang-Rhys vibrational mode [2] at thermal equilibrium yields coherence times which are slightly shorter than experimentally observed [15]. On the basis of Redfield-type approaches, it has been shown that the energy transfer is optimized when the parameters are chosen in the crossover regime between the overdamped and fully coherent dynamics [16–18]. When the energy gaps of the excitonic transitions are much larger than typical environmental fluctuational frequencies, relaxation is suppressed [10] and seemingly too weak to reach the optimal crossover regime [19]. However, discrete vibrational modes in the environmental spectrum, which are in resonance with excitonic energy differences, then can promote the corresponding transitions and thus the overall energy transfer [19–22]. However, this mechanism is not at play in the FMO complex.

Recently, it has been proposed that underdamped coherent low-frequency vibrations, which are strongly coupled to the electronic transitions and which are close to resonance, are responsible for the observed long-lived coherence [23–26]. The prominent vibrational mode with a wave number of 180 cm^{-1} has been explicitly included in the system's quantum dynamics such that this vibrational mode is included on an equal footing as the excitonic states. At the same time, a possible functional relevance of such an underdamped low-frequency vibration has not been studied so far. Underdamped high-frequency vibration have been shown to improve energy transfer in allophycocyanin [27]. Moreover, it has been realized that a coherent vibronic coupling strongly supports the charge transfer in organic photovoltaic blends [28].

In this paper, we reveal the constructive role of an underdamped vibrational mode on the coherent exciton transfer and its efficiency in the FMO complex. This becomes apparent from numerically exact results for the full FMO monomer with seven sites, the spectral density of Refs. [13,14] as extracted from measured optical spectra [13], and by including the dominant underdamped vibrational mode with the wave number 180 cm^{-1} explicitly in the *system*

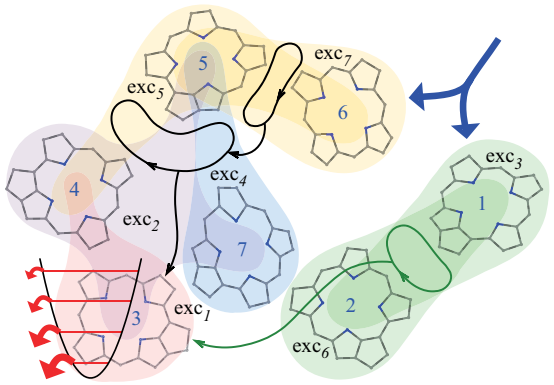

FIG. 1. (Color online) Structural arrangement of the seven main BChl molecules in the FMO complex (*Chlorobium tepidum*) superposed with a schematic representation of the delocalized excitons (color shading). The two main excitation transfer passageways are indicated by the thin arrows. The harmonic oscillator parabola highlights the underdamped molecular vibrations which speeds up the energy transfer.

Hamiltonian, thereby assuming it would be underdamped as recently proposed [23–26]. Employing the iterative real-time quasiadiabatic propagator path integral (QUAPI) [29–32], we quantitatively show that such an underdamped vibrational mode generates additional quantum coherent transfer channels such that the excitation energy is funnelled most efficiently through the FMO molecular aggregate under realistic physiological conditions. We find a substantial reduction of the transfer times of up to 24%, as compared to the complex without this vibrational mode and, most importantly, also as compared to the dynamics with an overdamped 180-cm^{-1} mode treated as a broad peak in the environmental spectral function.

II. MODEL

A. Excitonic Hamiltonian

The FMO monomer contains eight bacteriochlorophyll *a* (BChl*a*) molecular sites [8], of which the recently discovered eighth pigment [33,34] is only weakly coupled to the other BChls and thus will be omitted in the following. The Hamiltonian restricted to the single excitation subspace for the remaining seven sites is $H_{\rm FMO} = \sum_{j=1}^{7} \epsilon_j |j\rangle\langle j| + \sum_{j\neq k} J_{jk} (|j\rangle\langle k| + |k\rangle\langle j|)$, where the basis states $|j\rangle$ indicate that the j-th site is in its excited state and all other sites are in their ground states. ϵ_j denotes the energy of the j-th site and J_{jk} the electronic coupling between sites j and k. We use the numerically determined site energies and dipolar couplings of *Chlorobium tepidum* [14] (in units of cm^{-1}),

$$H_{\rm FMO} = \begin{pmatrix} 240 & -87.7 & 5.5 & -5.9 & 6.7 & -13.7 & -9.9 \\ & 315 & 30.8 & 8.2 & 0.7 & 11.8 & 4.3 \\ & & 0 & -53.5 & -2.2 & -9.6 & 6.0 \\ & & & 130 & -70.7 & -17.0 & -63.3 \\ & & & & 285 & 81.1 & -1.3 \\ & & & & & 435 & 39.7 \\ & & & & & & 245 \end{pmatrix}. \quad (1)$$

The BChl 3 is the site with the lowest energy. It is connected to the RC and forms the exit site [8] out of the FMO complex. BChls 1 and 6 are oriented towards the baseplate protein [8]. These sites are therefore considered as the entrance sites, which are initially populated.

B. Environmental fluctuations

The surrounding vibrational pigment-protein-solvent environment induces thermal polar fluctuations on the excitation transfer dynamics. We treat the electronic states of the FMO complex within an open quantum system approach [35]. The Gaussian thermal fluctuations are generated by environmental harmonic modes [2] and the total Hamiltonian thus is

$$H = H_{\rm FMO} + \sum_{j=1}^{7} \frac{1}{2} \sum_{\alpha} \left(p_{j,\alpha}^2 + \omega_{j,\alpha}^2 q_{j,\alpha}^2\right) + \sum_{j=1}^{7} |j\rangle\langle j| \sum_{\alpha} \kappa_{\alpha}^{(j)} q_{j,\alpha}$$

with momenta $p_{j,\alpha}$, displacements $q_{j,\alpha}$, frequencies $\omega_{j,\alpha}$, and coupling constants $\kappa_{\alpha}^{(j)}$ of the environmental fluctuations at site j. We assume that the fluctuations at different BChl sites are identical in their characteristics but spatially uncorrelated [15]. The environmental fluctuations and their coupling to the system dynamics are characterized by their spectral density,

$$G(\omega) = \sum_{j,\alpha} \left(\left|\kappa_{\alpha}^{(j)}\right|^2 / 2\omega_{j,\alpha}\right) \delta(\omega - \omega_{j,\alpha}),$$

which determines the temporal correlations of the environmental fluctuating forces and thus the relaxation and dephasing behavior [35]. Here we use the experimentally determined [13] and theoretically parametrized [14,36] functional form $G(\omega) = S_0 g_0(\omega) + S_H \omega^2 \delta(\omega - \omega_H)$. This fluctuational spectrum contains both a broad low-frequency contribution $S_0 g_0(\omega)$ by the protein vibrations with Huang-Rhys factor S_0 and a single effective vibrational mode of the pigments centered at $\omega_H = 180$ cm^{-1} with the Huang-Rhys factor $S_H = 0.027$ [13]. Wendling *et al.* [13] have identified up to 30 vibrational modes in their experimental data. The relevant

effective mode at 180 cm^{-1} in fact consists of three strongly overlapping vibrational modes at 173 cm^{-1}, 185 cm^{-1}, and 195 cm^{-1}. Following Wendling *et al.* [13], we combine the weights of the three modes around 180 cm^{-1} out of the 30 modes to an effective mode with Huang-Rhys factor $S_H = 0.027$. Then we neglect all other specific vibrational modes.

For the broad low-frequency background, we follow Adolphs and Renger [14] and use a functional form originally determined for B777 complexes [37]. It is given by

$$g_0(\omega) = (6.105 \times 10^{-5})\frac{\omega^5}{\omega_1^4}\exp\left[-\sqrt{\frac{\omega}{\omega_1}}\right] + (3.8156 \times 10^{-5})\frac{\omega^5}{\omega_2^4}\exp\left[-\sqrt{\frac{\omega}{\omega_2}}\right], \quad (2)$$

with $\omega_1 = 0.575\ \mathrm{cm}^{-1}$ and $\omega_2 = 2\ \mathrm{cm}^{-1}$. The Huang-Rhys factor $S_0 = 0.5$ was estimated from the temperature dependence of the absorption spectra of FMO complexes [13].

C. Treatment of the discrete 180-cm^{-1} vibrational mode

In general, within the system-bath approach, the environment is commonly assumed to be in a thermal equilibrium state. Thus, including a discrete vibrational mode into the environmental spectrum implicitly assumes that the discrete mode only fluctuates thermally around its equilibrium state, although with a possibly finite correlation time. When the 180-cm^{-1} mode is underdamped and included via a δ peak in $G(\omega)$, it induces in principle infinitely long oscillatory correlations [35]. A finite relaxation in this vibrational mode renders the correlation time finite, but it still can be rather long. A system-bath approach yields correct results when it is able to treat these long-time correlations, which is typically not practical. It is more convenient (and equivalent [38]) to include the vibrational molecular mode at 180 cm^{-1} explicitly as part of the *system* Hamiltonian and remove it from $G(\omega)$ accordingly. This furthermore allows energy exchange not only from the excitonic part into this mode but also backwards. Specifically, the energy transfer back from the mode into the excitonic system is excluded when treating the environment as a set of infinite harmonic degrees of freedom.

To reveal the importance of the underdamped mode for the global transfer time, we compare three cases: (i) First, we entirely omit the discrete mode, i.e., $S_H = 0$; (ii) second, we treat the mode as part of the environmental spectrum, i.e., assume that it evolves close to its thermal equilibrium; and, (iii) third, we include it explicitly as part of the *system* Hamiltonian [and then removing it from the spectrum $G(\omega)$]. When including the mode into the environmental spectrum [case (ii)], we in addition assume that due to the surrounding environment, the vibrational mode itself is strongly damped. This leads to a finite broadening of the mode in the spectral density [15,39], i.e., to a Lorentzian line shape. We choose the width $\gamma = 29\ \mathrm{cm}^{-1}$ in the form $S_H\omega^2\delta(\omega-\omega_H) \to S_H\omega_H\gamma\omega^2/[(\omega-\omega_H)^2+\gamma^2]$.

Separating the mode from the environment to treat it as part of the system results in a Hamiltonian $H = H_{\mathrm{FMO,vib}} + H'_{SB}$ with

$$H_{\mathrm{FMO,vib}} = H_{\mathrm{FMO}} + \sum_{j=1}^{7}\left[|j\rangle\langle j|\kappa_H^{(j)}q_{j,H} + \frac{1}{2}\left(p_{j,H}^2 + \omega_{j,H}^2 q_{j,H}^2\right)\right],$$

where H'_{SB} is the system-bath part excluding the discrete 180-cm^{-1} mode from the environmental spectrum.

In order to obtain a numerically tractable model, we will restrict the Hilbert space of the seven 180-cm^{-1} modes (one at each chromophore) to include only a finite number of vibrational excitations. This gives rise to the effective system Hamiltonian

$$H_{\mathrm{FMO,vib}} = H_{\mathrm{FMO}} + \sum_{j=1}^{7}\sum_{\nu_j=0}^{\nu_{j,\max}}\nu_j\hbar\omega_H|\nu_j\rangle\langle\nu_j| + \sum_{j=1}^{7}|j\rangle\langle j|\sum_{\nu_j=1}^{\nu_{j,\max}}\lambda_{\nu_j}\{|\nu_j-1\rangle\langle\nu_j| + |\nu_j\rangle\langle\nu_j-1|\}$$

with $\lambda_{\nu_j} = \sqrt{\nu_j}\hbar\omega_H S_H$.

Due to the exponential growth of the computer power required for QUAPI with the increasing system size, we need to restrict our model further. In detail, we consider, on the one hand, the discrete 180-cm^{-1} mode at one site only, i.e., setting $\nu_{j,\max} = 1$ for a single site j and all others to zero. On the other hand, within our maximal model (which is used unless stated otherwise), we include only those vibrational states of that site where an exciton is created. Formally, we thus take only those states $|j,\nu_j,\nu_{i\neq j} = 0\rangle$ into account and restrict the Hilbert space of the total system to basis states with corresponding energies up to 450 cm^{-1}. By this, we exclude states with higher energies whose occupations are exponentially suppressed at room temperature. The former step neglects states which are almost degenerate with the vibrationally excited states which are included. Since each exciton state is equally degenerate due to the vibrational states, this simplification will not change the relative population dynamics of the pigment sites qualitatively. In order to treat the energy transfer in this restricted model consistently, we assume dipolar couplings $J_{(i,\nu_i),(j,\nu_j)} = J_{i,j}$. As a test, we have also simulated the transfer dynamics with dipolar couplings $J_{(i,\nu_i\neq 0),(j,\nu_j\neq 0)} = 0$. This yields similar transfer times. We note that our focus is on the qualitative influence of underdamped vibrational modes in an exactly treated biomolecular environment instead of a more comprehensive model treated within a Refield-type approach. To be explicit, we incorporate in our maximal model the states $|j,\nu_j\rangle$ with

$$|1,0\rangle,|2,0\rangle,|3,0\rangle,|4,0\rangle,|5,0\rangle,|6,0\rangle,|7,0\rangle$$
$$|1,1\rangle,|4,1\rangle,|7,1\rangle,|3,1\rangle,|3,2\rangle.$$

D. Modeling the energy transfer towards the reaction center

In order to discuss the efficiency of the energy transfer through the FMO complex towards the RC, we model the latter as an incoherent energy sink which is connected solely to site 3 [16–18]. Thus, we include another state $|\mathrm{RC}\rangle$ and the transfer towards the RC state is treated as an incoherent population decay on a purely phenomenological level. The associated

decay rate $\Gamma_{\rm RC} = 1\,{\rm ps}^{-1}$ is assumed as constant, since we are not interested in the explicit details of the dumping process. We study the influence of underdamped modes on the energy transfer towards the reaction center. Backtransfer from the RC to the FMO complex is thereby excluded. In turn, the rise time of the population growth of the RC is taken as a measure for the efficiency of the energy transfer through the complex.

To be specific, the quantum statistical dynamics is formally treated within an effective master equation for the total statistical operator W which includes the FMO complex, its Gaussian environment, and the occupation of the reaction center $\rho_{\rm RC} = |{\rm RC}\rangle\langle{\rm RC}|$. The technical form is given by

$$\partial_t W = -\frac{i}{\hbar}[H,W] - \Gamma_{\rm RC}\sum_{\nu_3}|3,\nu_3\rangle\langle 3,\nu_3|$$

$$\partial_t \rho_{\rm RC} = \Gamma_{\rm RC}\sum_{\nu_3}|3,\nu_3\rangle\langle 3,\nu_3|.$$

The dynamics where the system-bath coupling is involved is simulated by employing the QUAPI scheme [29–32,40] calculating the time-dependent reduced density operator. It evaluates the dissipative path integral iteratively and is by construction numerically exact, such as the hierachy equation of motion approach [41]. It has been verified against exactly solvable models [30] and compared to the cumulant time-nonlocal master equation approach [11].

III. RESULTS

To pinpoint the influence of localized vibrational molecular modes on the transfer efficiency, we determine the excitonic dynamics at room temperature with the 180-cm^{-1} mode being included in the system Hamiltonian. Figure 2 shows the corresponding time-dependent population $\rho_{\rm RC}(t)$ of the energy sink (blue/upper full line) for two different initial conditions, i.e., $\rho_{11}(0) = |\langle 1,0|1,0\rangle|^2 = 1$ (left) and $\rho_{66}(0) = |\langle 6,0|6,0\rangle|^2 = 1$ (right), with the vibrational mode being initially in the ground

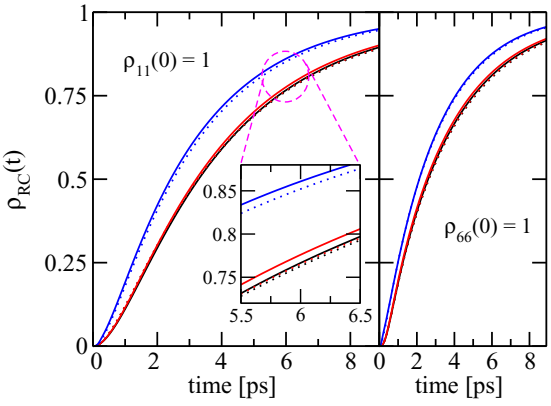

FIG. 2. (Color online) Time-dependent increase of the FMO reaction center (RC) population at room temperature for (left) $\rho_{11}(0) = 1$ and (right) $\rho_{66}(0) = 1$ for the cases when the 180-cm^{-1} molecular vibrational mode is underdamped [blue (upper) lines], strongly damped [red (lower) lines], and omitted from the model (black lines on top of the red lines). The dotted lines mark the sink populations when the Huang-Rhys factor S_0 is increased by a factor of 2, see text.

state. We have obtained similar results when starting from vibrationally excited states (not shown). The population of the energy sink increases in a monotonous manner. We use the rise time of the exponential growth of $\rho_{\rm RC}(t)$ as a measure for the efficiency and refer to it as "transfer time" in short. The observed transfer time is 2.9 ps for $\rho_{11}(0) = 1$ and 2.8 ps for $\rho_{66}(0) = 1$ at $T = 300$ K. In contrast to the underdamped vibrational mode, a strongly damped 180-cm^{-1} molecular vibrational mode generates a considerably slower rise of the sink population and much longer transfer times, see the red (lower) full lines in Fig. 2. The result for this case is transfer times of 3.8 and 3.4 ps. Interestingly, when the 180-cm^{-1} mode is completely omitted in the model, roughly the same transfer dynamics and times (black lines in Fig. 2) follow. Thus, only a molecular underdamped vibrational mode is able to reduce the energy transfer times by about 24% for $\rho_{11}(0) = 1$ and 18% for $\rho_{66}(0) = 1$ in the FMO. The speed-up is slightly more pronounced when the initial excitation starts at site 1, since the transfer starting at site 6 is already faster than that starting at site 1 when no vibrational mode is present [7]. Note that an overall speed-up of about 24% is rather significant.

The observed considerable vibronic speed-up cannot be explained by a mechanism as introduced by Kolli *et al.* [19] and del Ray *et al.* [21], since it only occurs when the 180-cm^{-1} molecular vibrational mode is treated as part of the system. It does not occur for a strongly damped mode initially at thermal equilibrium and thus as part of the environmental fluctuations spectrum as in Refs. [19,21].

To further elucidate the detailed mechanism by which the vibrations enhance the transfer efficiency (and the coherence times), we study next the excitonic dynamics by coupling the 180-cm^{-1} molecular vibrational mode only at selected sites and omitting it for respective other sites. In particular, we consider two cases: First, the vibrational mode is coupled to the entrance site 1. For this configuration, we observe prolonged transfer times of 4.1 ps for $\rho_{11}(0) = 1$ and 3.6 ps for $\rho_{66}(0) = 1$. Second, and in contrast to this, when we couple the mode to exit site 3 only, we observe shorter transfer times of 2.7 ps for $\rho_{11}(0) = 1$ and 2.6 ps for $\rho_{66}(0) = 1$. Hence, the observed vibronic speed-up is directly linked to the quantum dynamics of the vibrational mode at *exit* site 3 (the *quantum exit*). We obtain the appealing and simple picture that the quantum coherent vibrational states add additional efficient exit pathways in form of additionally decay channels into the RC. Accordingly, for a quantum coherent mode, many more quantum states are connected to the RC and are available to become populated during the exciton transfer in the complex. Consequently, more quantum states can dump their energy into the sink. The total population of the sink then can grow faster, which yields an overall increased transfer efficiency. In contrast to the quantum dumping of energy into the RC by the quantum exit, additional vibrational states at sites other than the exit site tend to significantly decrease the transfer efficiency. They provide additional intermittent states for the transfer in which the energy is intermittently stored without connection to the RC and thus is stuck. This reduces the overall transfer efficiency. All resulting energy transfer times at $T = 300$ K are summarized in Table I.

The explicit treatment of the quantum dynamics of the 180-cm^{-1} mode was recently proposed [23–26] to

TABLE I. Excitation energy transfer times at $T = 300$ K without and with underdamped vibrational modes coupled to the pigment sites. A negative change in the transfer time indicates a speed-up, while a positive sign indicates a slower transfer as compared to the case without vibrational states.

Vibrational mode coupled to	Initial excitation at site	Transfer time (ps)	Change by
NO vibration	1	3.8	–
	6	3.4	–
All sites	1	2.9	−24 %
	6	2.8	−18 %
Site 1	1	4.1	+8 %
	6	3.6	+6 %
Site 3	1	2.7	−29 %
	6	2.6	−24 %

understand and describe the experimentally observed long-lived quantum coherence in the FMO complex. For our more-accurate modeling of the environmental fluctuations by the physical spectral density, our numerically exact results also yield an enlarged time window (as compared to a strongly damped vibrational mode) with an oscillatory dynamics of the populations when the 180-cm^{-1} mode is included as part of the system dynamics. Exciting initially site 1, i.e., $\rho_{11}(0) = 1$, we find a coherent population transfer among site 1, site 2 (both in the vibrational ground state, i.e., states $|1,0\rangle$ and $|2,0\rangle$), and the first vibrationally excited state on site 1, i.e., $|1,1\rangle$. The corresponding populations are denoted as ρ_{11}, ρ_{22}, and ρ_{vib1}, respectively. Their time evolution is plotted in Fig. 3 (full lines). We extract coherence times of about 300 fs for $T = 300$ K. The dashed lines in Fig. 3 show the population dynamics of sites 1 and 2 when omitting the 180-cm^{-1} mode

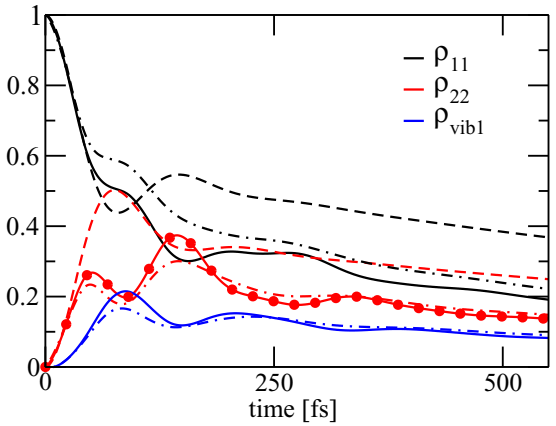

FIG. 3. (Color online) Time-dependent populations time of site 1, site 2 (both in the vibrational ground state), and the first vibrationally excited state on site 1. The full lines refer to the full treatment of the 180-cm^{-1} mode as part of the system, while the dashed lines mark the case when the 180-cm^{-1} mode is omitted. The dash-dotted lines refer to the case of the Huang-Rhys factor S_0 increased by a factor of 2. All lines show spline polynomials fitted to the data as guide for the eyes, which, for clarity, are shown by red full circles for the full red line only.

completely. The absence of the vibrational mode clearly leads to a shorter coherence time.

In order to elucidate any connection between the observed prolonged coherent population dynamics and the energy transfer speed-up, we next consider the case when the 180-cm^{-1} mode is treated as part of the system but with the environmental fluctuations strength S_0 increased by a factor of 2, i.e., $S_0 \to 2S_0$. The results are given by the dash-dotted lines in Fig. 3. We find clearly reduced oscillation amplitudes and coherence times as expected for a more strongly damped configuration. However, the associated time-dependent growth of the sink population shows no noticeable difference when compared to the original situation with a smaller Huang-Rhys factor S_0. This is shown in Fig. 2 by the dotted line, see the inset for better distinguishability of full and dotted lines. Overall, the underdamped modes at 180 cm^{-1} clearly improve the efficiency of the quantum coherent energy transfer and, at the same time, result in the observed prolonged quantum coherent oscillations. Both are the result of the dynamics of the vibrational modes, which do not thermalize on fast time scales compared to the electronic energy transfer dynamics. Beyond that, the speed-up of the energy transfer seems rather insensitive to the actual coherence lifetimes.

IV. CONCLUSION

Our numerically exact results for the real-time nonequilibrium quantum dynamics of the excitation energy transfer through the FMO complex in the presence of physically realistic environmental fluctuations show that additional underdamped localized molecular vibrational modes at 180 cm^{-1} can play a significant role in increasing the transfer efficiency of this biological complex. We find a substantial speed-up of the transfer times of up to 24%, as compared to the complex without the 180-cm^{-1} mode and, most importantly, also compared to the complex with a strongly damped 180-cm^{-1} mode. The additional vibrationally coherent quantum states at exit site 3 are responsible for the speed-up as they provide additional transfer channels from the exit site to the reaction center. In contrast, vibrationally coherent states at sites other than the exit site tend to slow down the transfer since the energy is intermittently stuck. Prolonged coherence times in the complex resulting from the coupling of the underdamped vibrational modes seem not to be functionally necessary for the enormous speed-up of the transfer. Our results provide an amazingly simple strategy for optimizing artificial light-harvesting systems as well. Their global quantum transfer efficiency might be significantly increased by engineering the vibrational modes, with a particular focus on the exit site, without the need to increase the number of absorbing photoactive sites.

ACKNOWLEDGMENTS

We acknowledge financial support by the DFG SFB 925 “Light-induced dynamics and control of correlated quantum systems,” by the German Academic Exchange Service (DAAD), and by the DFG Excellence Cluster “The Hamburg Centre for Ultrafast Imaging - Structure, Dynamics and Control of Matter at the Atomic Scale.”

[1] H. van Amerongen, L. Valkunas, and R. van Grondelle, *Photosynthetic Excitons* (Singapore, World Scientific, 2000).

[2] V. May and O. Kühn, *Charge and Energy Transfer Dynamics in Molecular Systems*, 3rd ed. (Wiley-VCH, Weinheim, 2011).

[3] V. I. Novoderezhkin and R. van Grondelle, Phys. Chem. Chem. Phys. **12**, 7352 (2010).

[4] G. S. Engel, T. R. Calhoun, E. L. Read, T. K. Ahn, T. Mančal, Y.-C. Cheng, R. E. Blankenship, and G. R. Fleming, Nature **446**, 782 (2007).

[5] G. Panitchayangkoon, D. Hayes, K. A. Fransted, J. R. Caram, E. Harel, J. Wen, R. E. Blankenship, and G. S. Engel, Proc. Natl. Acad. Sci. U.S.A. **107**, 12766 (2010).

[6] B. Matthews, R. Fenna, M. Bolognesi, M. Schmid, and J. Olson, J. Mol. Biol. **131**, 259 (1979).

[7] T. Brixner, J. Stenger, H. Vaswani, M. Cho, R. E. Blankenship, and G. Fleming, Nature **434**, 625 (2005).

[8] M. T. W. Milder, B. Brüggemann, R. van Grondelle, and J. L. Herek, Photosynth. Res. **104**, 257 (2010).

[9] A. Ishizaki and G. R. Fleming, J. Chem. Phys. **130**, 234110 (2009).

[10] P. Nalbach and M. Thorwart, J. Chem. Phys. **132**, 194111 (2010).

[11] P. Nalbach, A. Ishizaki, G. R. Fleming, and M. Thorwart, New J. Phys. **13**, 063040 (2011).

[12] C. A. Mujica-Martinez, P. Nalbach, and M. Thorwart, Phys. Rev. E **88**, 062719 (2013).

[13] M. Wendling, T. Pullerits, M. A. Przyjalgowski, S. I. E. Vulto, T. J. Aartsma, R. van Grondelle, and H. van Amerongen, J. Phys. Chem. B **104**, 5825 (2000).

[14] J. Adolphs and T. Renger, Biophys. J. **91**, 2778 (2006).

[15] P. Nalbach, D. Braun, and M. Thorwart, Phys. Rev. E **84**, 041926 (2011).

[16] M. Mohseni, P. Rebentrost, S. Lloyd, and A. Aspuru-Guzik, J. Chem. Phys. **129**, 174106 (2008).

[17] A. Olaya-Castro, C. F. Lee, F. F. Olsen, and N. F. Johnson, Phys. Rev. B **78**, 085115 (2008).

[18] M. B. Plenio and S. F. Huelga, New J. Phys. **10**, 113019 (2008).

[19] A. Kolli, E. J. O'Reilly, G. D. Scholes, and A. Olaya-Castro, J. Chem. Phys. **137**, 174109 (2012).

[20] G. Ritschel, J. Roden, W. T. Strunz, and A. Eisfeld, New J. Phys. **13**, 113034 (2011).

[21] M. del Rey, A. W. Chin, S. F. Huelga, and M. Plenio, J. Phys. Chem. Lett. **4**, 903 (2013).

[22] E. J. O'Reilly and A. Olaya-Castro, Nat. Commun. **5**, 3012 (2014).

[23] N. Christensson, H. F. Kauffmann, T. Pullerits, and T. Mančal, J. Phys. Chem. B **116**, 7449 (2012).

[24] T. Mančal, N. Christensson, V. Lukeš, F. Milota, O. Bixner, H. F. Kauffmann, and J. Hauer, J. Phys. Chem. Lett. **3**, 1497 (2012).

[25] V. Tiwari, W. K. Peters, and D. M. Jonas, Proc. Natl. Acad. Sci. U.S.A. **110**, 1203 (2013).

[26] A. W. Chin, J. Prior, R. Rosenbach, F. Caycedo-Soler, S. F. Huelga, and M. B. Plenio, Nat. Phys. **9**, 113 (2013).

[27] J. M. Womick and A. M. Moran, J. Phys. Chem. B **115**, 1347 (2011).

[28] S. M. Falke, C. A. Rozzi, D. Brida, M. Maiuri, M. Amato, E. Sommer, A. De Sio, A. Rubio, G. Cerullo, E. Molinari, and C. Lienau, Science **344**, 1001 (2014).

[29] N. Makri and D. E. Makarov, J. Chem. Phys. **102**, 4600 (1995); **102**, 4611 (1995).

[30] N. Makri, J. Math. Phys. **36**, 2430 (1995).

[31] M. Thorwart, P. Reimann, P. Jung, and R. F. Fox, Chem. Phys. **235**, 61 (1998).

[32] C. A. Mujica-Martinez, P. Nalbach, and M. Thorwart, Phys. Rev. Lett. **111**, 016802 (2013).

[33] D. E. Tronrud, J. Wen, L. Gay, and R. E. Blankenship, Photosynth. Res. **100**, 79 (2009).

[34] M. Schmidtam Busch, F. Müh, M. El-Amine Madjet, and T. Renger, J. Phys. Chem. Lett. **2**, 93 (2011).

[35] U. Weiss, *Quantum Dissipative Systems*, 3rd ed. (World Scientific, Singapore, 2008).

[36] Note that $G(\omega) = \omega^2 J(\omega)$ with $J(\omega)$ from Eq. (25) in Ref. [14].

[37] T. Renger and R. A. Marcus, J. Chem. Phys. **116**, 9997 (2002).

[38] A. Garg, J. N. Onuchic, and V. Ambegaokar, J. Chem. Phys. **83**, 4491 (1985).

[39] C. Olbrich and U. Kleinekathöfer, J. Phys. Chem. B **114**, 12427 (2010).

[40] Technical details of how to combine the master equation dynamics with the QUAPI approach will be presented elsewhere.

[41] Y. Tanimura, J. Phys. Soc. Jpn. **75**, 082001 (2006).